RSC Advances

PAPER

View Article Online
View Journal | View Issue

Check for updates

Cite this: *RSC Adv.*, 2017, **7**, 28898

The structure, electrical properties and chemical stability of porous Nb-doped $SrTiO_3$ – experimental and theoretical studies†

Ewa Drożdż * and Andrzej Koleżyński

A series of porous $SrTi_{1-x}Nb_xO_3$ samples (with $x = 0$, 1, 2 and 3 mol%) were prepared by wet synthesis and sintered at 1573 K. Single phase samples were obtained for each composition, as confirmed by XRD measurements. For all samples, aging tests in CO_2/H_2O atmosphere and electrochemical impedance spectroscopy measurements in air and hydrogen (reduced) atmosphere were carried out. Simultaneously, for model superstructures corresponding to 2 and 3 mol% experimental compositions, FP-LAPW DFT calculations of electronic structure and bonding properties (using QTAiM approach) were performed. Both experimental and theoretical results show an increase of cell parameters with increasing niobium amount. The influence of the amount of niobium on the microstructure of the synthesized samples as well as on their chemical stability was also observed. Electrical properties measurements showed different conduction mechanism for synthetic air and reduced atmosphere, *i.e.* mixed ionic-electron conduction and dominating electron conduction, respectively.

Received 13th April 2017
Accepted 24th May 2017

DOI: 10.1039/c7ra04205a

rsc.li/rsc-advances

Open Access Article. Published on 01 June 2017. Downloaded on 2/11/2026 10:26:06 AM.
This article is licensed under a Creative Commons Attribution-NonCommercial 3.0 Unported Licence.

Introduction

$SrTiO_3$ is one of the best known and most widely used perovskite materials with interesting properties primarily resulting from structure doping with aliovalent additives. Nowadays, the studies devoted to its potential use, among others, as materials for energy conversion (therein mixed ionic-electronic conductors[1–3] and thermoelectric materials[4,5]) are becoming increasingly important from applicational viewpoint. The modification of various properties of $SrTiO_3$ material can be achieved by its carefully designed doping in one (or simultaneously both) cationic sublattices with various admixtures. A lot of papers have been devoted to studies on defects and electrical properties of bulk Nb–$SrTiO_3$ materials (*inter alia*[6–8]) but they concerned dense materials consisting of grains with at least micrometer sizes. Only a few papers [*e.g.*[9,10]] put stress on the microstructure (grain size and porosity) in the context of these properties. Abrantes *et al.*[9] observed, during evaluation of response time of Nb-doped materials in different atmospheres, that the transient response of very porous samples with 5 mol% Nb after suddenly changing from reducing to oxidizing conditions are much shorter than in the case of bulk ones. Thus dense materials react slowly to changes in the atmosphere, while in the porous materials respective changes are much faster (the diffusion time inside individual grains becomes even around six order of magnitude smaller). This information is valuable from applicational viewpoint – in the case of the solid–gas reactions, the porous microstructure provides large surface for the possible reaction. This makes porous Nb-doped $SrTiO_3$ very interesting materials from the viewpoint of its possible use as composite component for SOFC anodes or oxide membranes in gas sensors (*e.g.* it is well known that in the case of SOFC materials the most important factor is the amount/effective area of TPB – Triple Phase Boundaries, directly related to porosity level which is required to be higher than 30 vol% and grain size which has to be nanosized).

The drawback of expanded surface materials is, however, an increase of the yield of competitive, disturbing reactions. One of the fundamental property of this type of perovskite materials is their pure stability in atmosphere containing carbon dioxide and water vapor.[11–13] This factor is especially important for materials that would potentially work in hydrocarbon environment due to a possibility of oxidation of organic carbon to carbon dioxide. Compared to ceranes, titanates, they exhibit higher chemical stability (in CO_2 and H_2O atmosphere) and, what is more, strontium titanate is one of the most stable representatives of this perovskite group. To our best knowledge, the effect of aliovalent dopant introduction to titanium sublattice on chemical stability of $SrTiO_3$ in the presence of CO_2/H_2O has not been studied so far. On the other hand, the only study on introduction of donor dopant to strontium sub-lattice showed that substituting strontium with yttrium does not lower the chemical stability of strontium titanate.[14] Analogous studies on donor doping influence on chemical stability were

AGH University of Science and Technology, Faculty of Materials Science and Ceramics, al. A. Mickiewicza 30, 30-059 Kraków, Poland. E-mail: edrozdz@agh.edu.pl; Fax: +48 12 617 52 36; Tel: +48 12 617 25 37

† Electronic supplementary information (ESI) available. See DOI: 10.1039/c7ra04205a

This journal is © The Royal Society of Chemistry 2017

Open Access Article. Published on 01 June 2017. Downloaded on 2/11/2026 10:26:06 AM.
This article is licensed under a Creative Commons Attribution-NonCommercial 3.0 Unported Licence.

conducted with respect to other perovskite systems (cobaltite,[15] ferrite[16]) and their results indicate that the niobium dopant in B sublattice stabilizes such systems. The authors of these works took into consideration thermodynamical aspect of niobium addition based on average metal–oxygen bond energy (ABE). The idea of such calculations (ABE) was originally proposed by Voorhoeve *et al.*[17] to estimate the binding energy of oxygen with metal ions in perovskite oxides.

There are also many theoretical studies reported in literature (based on both, DFT and HF calculations), devoted to various properties of niobium doped $SrTiO_3$ materials. One can find theoretical papers analyzing structural, electrical and catalytic properties of doped and undoped perovskite structures, including Nb-doped strontium titanate.[18–21] Based on various computational methods, insulator to metal transition, the position of Nb dopants (Ti, Sr or interstitial initial sites) within Nb-doped $SrTiO_3$ structure, partial ionic charges and unit cell size dependence on dopant as well as doping mechanism and properties and formation energies of substitutional or vacancy defects and dependence of electrical and optical properties on point defects has been studied.[22–28]

Most of theoretical papers devoted to electrical properties of Nb-doped $SrTiO_3$ contain detailed analysis of electronic structure properties (DOS and bandstructure).[22,23,29] However, these papers were concerned with some heavy doping models (high niobium concentrations), most probably due to prohibitive requirements for computer power in the case of big supercell calculations, necessary to model (low dopant concentration) and only recently, the calculations of electronic structure and optical properties for smaller niobium concentration (0.74–2.5 at% of niobium, corresponding to approx. 4–14 at% of titanium atoms substituted by niobium) has been reported.[28] Moreover, these works report some opposite findings, like *e.g.* opposite tendency of partial, charge transfer due to titanium substitution with niobium, towards oxygen or niobium[22,23] (HF or DFT ones).

Although Delugas *et al.*[29] stated that high-Nb doping concentration in $SrTiO_3$ are experimentally achievable and apparently keen to reach of high electron mobility, in practice, niobium concentration in titanium perovskite structures is limited to few per cents, due to interference with other phases being synthesized simultaneously, resulting in synthesis of multiphase, inhomogeneous materials.[6,30,31] Therefore much more realistic are the simulations of the systems with much lesser amount of doping agent. In this work, the results of WIEN2k FP-LAPW DFT calculations of electronic structure and topological properties of electron density, carried out for Nb doped $SrTiO_3$ model structures (for 0.42 at% and 0.56 at% of niobium, corresponding to approx. 2 mol% and 3 mol% of Ti substituted by Nb) and used in analysis of experimental results are presented.

Experimental

Synthesis

Porous undoped and Nb-doped $SrTiO_3$ materials were obtained by wet synthesis – sol–gel method. $Ti(O–iPr)_4$—titanium(IV) isopropoxide and niobium ethoxide were applied as precursors of titanium and niobium respectively. These two reagents were dissolved in anhydrous methanol and next cations were complexed by addition of citric acid. Then the aqueous solution of strontium nitrate (the concentration was confirmed by gravimetric analysis) was introduced into methanol solution containing titanium and niobium cations. The obtained sol was heated on magnetic stirrer at around 453 K until its densification (transition to a gel). After the calcination (1173 K) the pallets under pressure 5×10^5 Pa were formed and next sintered at 1573 K for 8 hours.

All reagents used for the synthesis were analytically pure (provided by Aldrich or Avantor Company).

A series of samples $SrTi_{1-x}Nb_xO_3$ where $x = 0$, 1, 2, 3 mol% were obtained and characterized.

Methods

Phase composition and unit cell parameters were determined based on XRD measurements carried out on Philips X'Pert Pro diffractometer with monochromatized Cu-Kα radiation for diffraction angles 2θ, within the range from 20 to 100. Using Rietveld phase analysis, the amounts of observed phases and crystallographic parameters were determined quantitatively. The crystallite sizes were estimated from the X-ray line broadening of the selected peaks, using Scherrer's approach.

The observation of pallets fracture morphology was performed using scanning electron microscopy (SEM) (Nova NanoSEM 200 FEI and Oxford Instruments) coupled with X-ray energy dispersive spectroscopy (EDAX company apparatus). The pallets porosity was measured using Archimedes method and specific surface by BET method.

The electrical properties of obtained samples were examined by means of impedance spectroscopy (Solartron, FRA 1260 with dielectric interface 1294). Before measurements, platinum paste was applied on the pallets (sintered at 1573 K, 10 mm in diameter and a thickness of 2.5 mm) and fired. The measurements were performed in temperature range of 573–973 K in synthetic air and mixture of 10% H_2 in Ar. The frequency range was 0.1 Hz–1 MHz and the amplitude of the sinusoidal voltage was 10 mV. Before the actual test the samples were initially annealed at hydrogen/argon atmosphere for 24 h (heated to 1023 K, kept at this temperature for an hour and then cooled to room temperature). Moreover, samples were equilibrated for 30 min at the specific temperature before actual EIS measurement.

In order to determine the chemical stability in CO_2 and H_2O atmosphere, the undoped and Nb-doped $SrTiO_3$ pallets were exposed to carbon dioxide and water vapour-containing atmosphere (7% CO_2 and 100% HR) for 700 h at room temperature. In order to check the stability of samples (original and subjected to aging procedure), thermogravimetric measurements (on SDT 2960 TA Instruments apparatus) coupled with mass spectroscopy (QMD 300 ThermoStar Balzers mass spectrometer) were used. All samples weighing around 50 mg were placed in SDT apparatus in platinum crucible and heated in synthetic air atmosphere with 10 deg min^{-1} heating rate.

Computational details

Ab initio calculations were carried out using Full Potential Augmented Plan Wave Method (FP-LAPW) within Density

Open Access Article. Published on 01 June 2017. Downloaded on 2/11/2026 10:26:06 AM.
This article is licensed under a Creative Commons Attribution-NonCommercial 3.0 Unported Licence.

Functional Theory formalism, as implemented in Wien2k package.[32] The calculations were carried out for three model structures: undoped $SrTiO_3$ and Nb-doped $SrTiO_3$ (with Nb/Ti ratio of 1/47 and 1/35), using $3 \times 3 \times 3$, $3 \times 4 \times 4$ and $3 \times 3 \times 4$ supercells, respectively, with single Ti atom substituted by niobium (the latter two correspond to nominal Nb content of 2 mol% and 3 mol%, respectively, comparable with the experimental ones). The calculations for 1 mol% Nb content were not carried out due to a very prohibitive time and memory requirements posed on supercomputer system by respective model supercell structure ($4 \times 5 \times 5$ supercell with 500 atoms and Nb/Ti ratio 1/99, where for even smaller RK_{max} parameter set to 5, single SCF cycle took many hours, while to obtain relaxed structure one needs to run many single point energy SCF calculations consisting of many cycles). Geometry optimization was performed by multi-step process (alternate equilibrium cell size determination for given atomic positions and atomic positions relaxation for fixed equilibrium unit cell size from previous step, until no further changes were observed) with following parameters: PBESol exchange correlation potential,[33] muffin-tin radii R_{MT} [a.u.]: 2.33 for strontium and 1.73 for titanium and niobium, $RK_{max} = 6.0$, $G_{max} = 14$, k-mesh: $6 \times 6 \times 6$, $5 \times 5 \times 6$ and $6 \times 6 \times 5$, for $SrTiO_3$, $SrTi_{0.98}Nb_{0.02}O_3$ and $SrTi_{0.97}Nb_{0.03}O_3$, respectively and the convergence criteria for SCF calculations set to $\Delta E_{SCF} \leq 10^{-5}$ Ry for total energy and $\Delta \rho_{SCF} \leq 10^{-5}$ e for electron density topology analysis. For all relaxed structures, the electronic structure (density of states and band structures) have been calculated and effective masses determined and Bader's QTAiM topological analysis[34] of total electron density carried out (using Critic2 (ref. 35) program).

Results & discussions

Structure and microstructure properties

The analysis of diffractograms obtained for $SrTi_{1-x}Nb_xO_3$ pallets sintered at 1573 K showed, in the case of all synthesized materials, the presence of cubic (space group *Pm3m*) $SrTiO_3$ phase only (Fig. 1).

Based on the comparison of ionic radii in 6-fold coordination (as is for B-cation in perovskite structure) for Ti(IV) and Nb(V), 74.5 pm and 78 pm, respectively, one can expect a slight increase of unit cell parameter with niobium substitution for titanium. The structural data determined using Rietveld method as well as theoretical calculations (details in next paragraph) confirmed the expected changes of cell parameters (Fig. 2). Furthermore, based on X-ray diffraction, using Scherrer equation, the crystallite sizes were calculated. As one can observe, there is a close relation between amount of introduced admixture and crystallite sizes (Fig. 2). With the addition of niobium, the mean crystallite size decreases and in the case of 3 mol% Nb-doped system reaches approx. half of the value assessed for the undoped material. The similar effect of grain size decrease with increasing amount of niobium introduced to $SrTiO_3$ structure was reported for dense samples sintered at 1800 K with much bigger grains.[36] The SEM microphotographs of pallets fractures obtained for our samples show porous materials with irregular pore structure (Fig. 3). The total

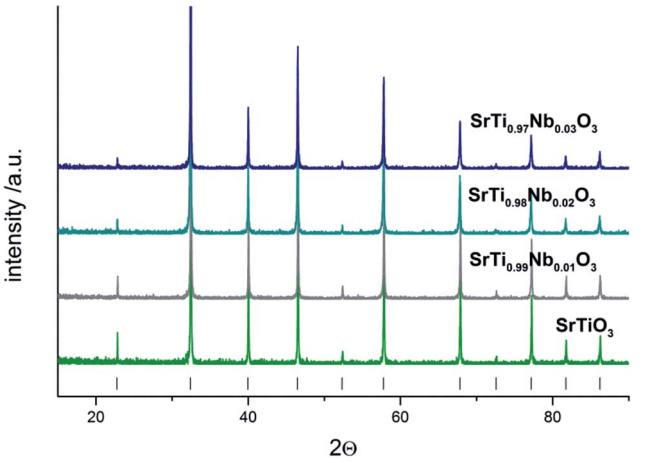

Fig. 1 Diffraction patterns of niobium doped $SrTiO_3$ samples sintered at 1573 K. The diffraction pattern of cubic $SrTiO_3$ from ICSD database (card no. 98-006-5089) is shown at the bottom of the drawing.

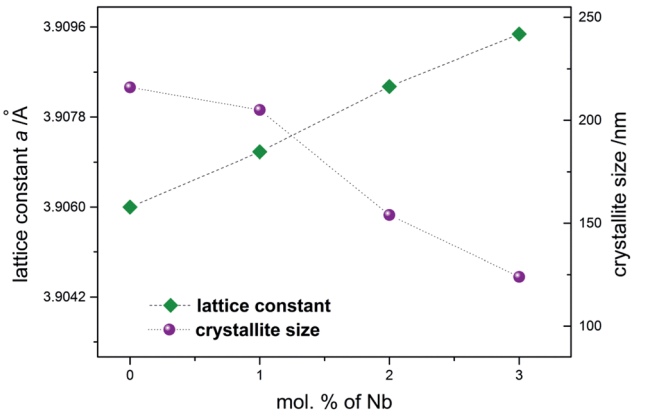

Fig. 2 Unit cell parameter and crystallite size as a function of the amount of niobium substituting titanium in $SrTiO_3$ samples.

porosities determined on the basis of geometric measurements and samples' weights were equal to 22 ± 3 vol%, BET surface area around 2.0 ± 0.4 m^2 g^{-1} and no dependency on the amount of niobium introduced was observed. The presence of niobium in the series of Nb-doped $SrTiO_3$ were confirmed by EDS microanalysis.

FP-LAPW DFT calculations

Crystal structure. The DFT FP-LAPW calculations were carried out for three model structures: undoped $SrTiO_3$ and two Nb-doped $SrTiO_3$ model structures using $3 \times 3 \times 3$ ($Pm\bar{3}m$, space group no. 221), $4 \times 4 \times 3$ ($P4/mmm$, sg no. 123) and $3 \times 3 \times 4$ ($P4/m$, sg. 83) supercells, respectively. In the latter two structures one titanium atom was substituted by niobium, which corresponds to 2.13 mol% and 2.86 mol% of titanium atoms substituted (0.42 at% and 0.56 at% wrt total number of atoms), respectively. The obtained results show (Fig. 4) that the unit cell size increases with increasing amount of niobium which is in agreement with the experimental results (Fig. 2).

This journal is © The Royal Society of Chemistry 2017

Open Access Article. Published on 01 June 2017. Downloaded on 2/11/2026 10:26:06 AM.
This article is licensed under a Creative Commons Attribution-NonCommercial 3.0 Unported Licence.

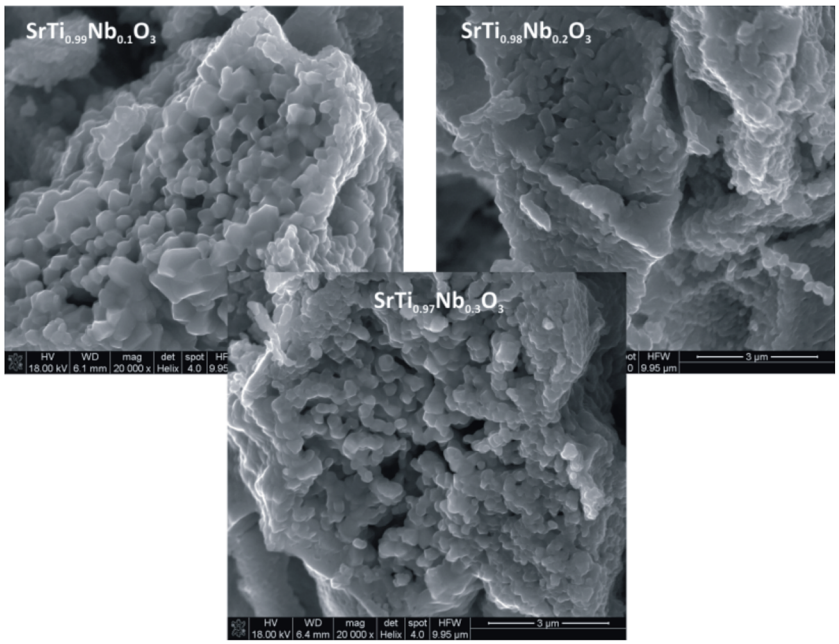

Fig. 3 SEM microphotographs of fractures of Nb-doped $SrTiO_3$ pallets (1, 2 and 3 mol% of Nb). All microphotographs were prepared at the same magnification (20 000×).

This is a direct result of local structure modification in niobium proximity: while niobium ions are only slightly bigger than titanium ones (78 *vs.* 74.5 pm), Nb–O bonds are visibly bigger than Ti–O bonds (~1.965 Å *vs.* ~1.95 Å, Table 2.) and so are their octahedra. Moreover, since niobium and titanium polyhedra are corner-shared, the increased length of Nb–O bonds leads to a shrinkage of respective Ti–O bonds and titanium polyhedra deformation. In the case of perovskite materials in order to determine the extent of polyhedral deformation one can use the so called polyhedra deformation indicators:[37–39] distortion index D, quadratic elongation $\langle\lambda\rangle$, bond angle variance σ^2 and effective coordination number ECoN (detailed description can be found in ESI†). The results of structural analysis based on the above descriptors are presented in Table 1 (only first two coordination spheres are shown, since 3rd coordination sphere with 8 titanium atoms has approx. 6.75 Å and 6.77 Å radius for 2 mol% and 3 mol% Nb-doped $SrTiO_3$, respectively, which is more than a half of the nearest distance between two niobium atoms in these structure, equal to 11.68 Å and 11.71 Å respectively). When we look closer at the detailed information about the properties of titanium octahedra in 1st and 2nd coordination sphere of niobium polyhedron (depicted on Fig. 5), we can observe that in both doped structures, 6 titanium polyhedra in 1st coordination sphere are visibly more distorted (octahedron elongation, bond length distortion, bond angle variance) than 12 belonging to 2nd coordination sphere, for which this distortion is almost negligible.

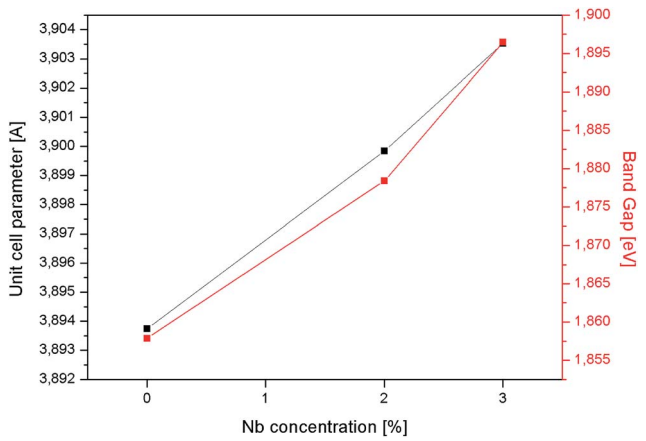

Fig. 4 Unit cell and band gap sizes calculated for undoped and 2 mol% and 3 mol% niobium doped $SrTiO_3$ optimized model superstructures (full geometry optimization, *i.e.* unit cell size and atomic position has been carried out).

Electron density topology. Based on the total electron densities obtained in FP-LAPW calculations for model structures, the topological analysis of electron density using Bader's QTAiM method was carried out and respective bond critical points (BCP) properties are presented in Table 2 (since there are many symmetrically nonequivalent atoms in unit cells of model structures and therefore also of BCPs, only average values are presented here). The obtained results show that all bonds have significant ionic character and Sr–O bonds are much weaker than Nb–O and Ti–O ones (several times lower charge concentration in bonding region) and thus they will be more prone to changes than bonds formed by B cations and titanium octahedra are slightly distorted (the further from niobium octahedron, the smaller distortion) in order to compensate B cation–oxygen bonds changes when niobium is introduced into $SrTiO_3$ structure.

Open Access Article. Published on 01 June 2017. Downloaded on 2/11/2026 10:26:06 AM.
This article is licensed under a Creative Commons Attribution-NonCommercial 3.0 Unported Licence.

Table 1 Structural properties of TiO_6 octahedra belonging to the first two niobium coordination spheres

$SrTi_{0.98}Nb_{0.02}O_3$			Nb–Nb distance: 11.67856 Å					
			TiO_6 octahedron					
Coord. sphere	No. of Ti atoms	Nb–Ti distance [Å]	Average bond length [Å]	Volume [Å^3]	Distortion index D (bond length)	Quadratic elongation <λ>	Bond angle variance σ^2 [deg^2]	Eff. coord. number
1	2	3.9263	1.9415	9.7541	0.0049	1.0003	0.8207	5.9878
	4	3.9387	1.9431	9.7751	0.0066	1.0005	1.5605	5.9747
2	8	5.5066	1.9474	9.8470	0.0010	1	0.0212	5.9997
	4	5.5076	1.9472	9.8436	0.0013	1	0.0251	5.9995
$SrTi_{0.97}Nb_{0.03}O_3$			Nb–Nb distance: 11.71069 Å					
			TiO_6 octahedron					
Coord. sphere	No. of Ti atoms	Nb–Ti distance [Å]	Average bond length [Å]	Volume [Å^3]	Distortion index D (bond length)	Quadratic elongation <λ>	Bond angle variance σ^2 [deg^2]	Eff. coord. number
1	4	3.9334	1.9480	9.8543	0.0045	1.0002	0.6124	5.9896
	2	3.9457	1.9493	9.8711	0.0061	1.0004	1.1804	5.9777
2	4	5.5220	1.9530	9.9326	0.0008	1	0.0063	5.9998
	8	5.5231	1.9528	9.9284	0.0012	1	0.0133	5.9996

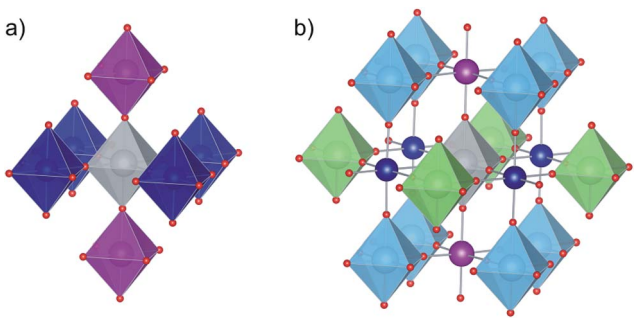

Fig. 5 (a) 1st and (b) 2nd niobium coordination spheres composed of titanium octahedra.

Electronic structure

Density of states. The results of electronic structure calculations carried out for model superstructures show (Fig. 6) that doping of strontium titanate with niobium substituting titanium results in a shift of Fermi level from band gap to conduction band (CB) and thus change of material to n-type semiconductor (donor doping), change of bands curvature close to CB minimum and valence band (VB) maximum (changes of carrier's effective masses – see details below) and slight increase of band gap size (Fig. 4) – for higher niobium amount Fermi level is shifted deeper into conduction band and band gap is wider. Presented results show that the states close to the top of VB are predominantly composed of oxygen 2p states. States close to the bottom of CB are predominantly composed of titanium 3d and niobium 4d states, divided into two distinct groups being reminiscent of the octahedral crystal field splitting into triple degenerate t_{2g} and doubly degenerate e_g groups (the former located at lower energies). Moreover, one can observe that the donor doping with niobium do not modify visibly states close to band gap (VB top and CB bottom) which are most important for electrical properties and results mostly in Fermi level shifting to CB (excess niobium electrons fill empty states with predominant d t_{2g} character) and small increase of bang gap with increasing amount of dopant. This indicates that one can safely use rigid band approximation for approximately assessing the changes in carrier concentration

Table 2 BCP properties calculated from the total electron density for niobium doped $SrTiO_3$ model structures, for two different niobium doping level (average values): bond length R and electron density $\rho(r_{BCP})$ and Laplacian $\nabla^2\rho(r_{BCP})$

mol% of Nb	R [Å]			$\rho(r_{BCP})$ [a.u.]			$\nabla^2\rho(r_{BCP})$ [a.u.]		
	Sr–O	Nb–O	Ti–O	Sr–O	Nb–O	Ti–O	Sr–O	Nb–O	Ti–O
0	2.750	—	1.947	0.0215	—	0.1088	0.0871	—	0.3895
2	2.753	1.964	1.946	0.0216	0.1378	0.1114	0.0864	0.3016	0.2458
3	2.760	1.965	1.951	0.0227	0.1286	0.1100	0.0876	0.2709	0.2462

This journal is © The Royal Society of Chemistry 2017

Open Access Article. Published on 01 June 2017. Downloaded on 2/11/2026 10:26:06 AM.
This article is licensed under a Creative Commons Attribution-NonCommercial 3.0 Unported Licence.

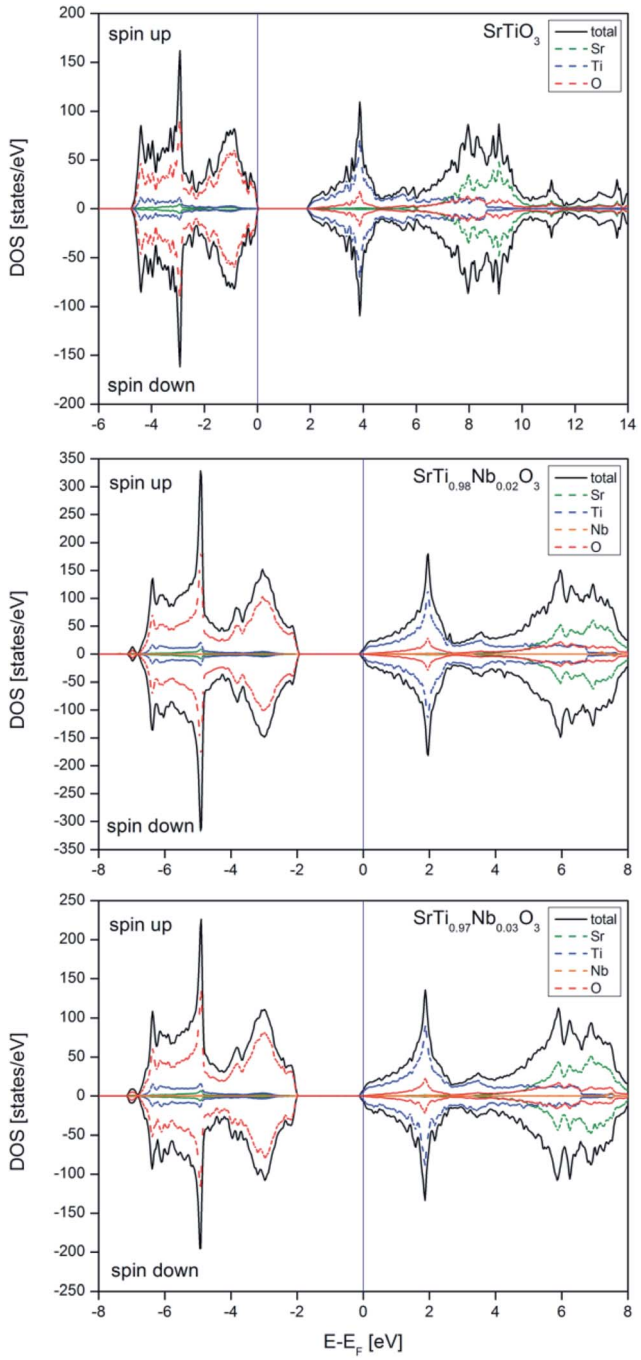

Fig. 6 Density of states (total and projected onto particular atoms) calculated for undoped (top), 2 mol% (middle) and 3 mol% (bottom) niobium doped $SrTiO_3$ optimized model superstructures.

and Fermi level position with changing amount of donor dopant.

Effective masses. Additional calculations were performed to estimate the effective masses of carriers near the band gap (a parabolic dispersion relationship was assumed). Since spin polarized calculations were carried out for model structures, the effective masses for three spin-up and spin down bands, closest to the extremum, were determined and the obtained results (in good agreement with previously reported for undoped and heavier Nb-doped $SrTiO_3$ (ref. 40 and 41)), together with their average values are presented in Table S1 in ESI.† It follows from these results that for niobium doped $SrTiO_3$ the effective masses for both holes and electrons increase, which indicates that niobium addition should decrease electric conductivity of doped material. However, while for holes this increase is significant and higher for bigger amount of admixture, for electrons the picture is slightly more complicated, since while effective masses of electrons in conduction bands close to Fermi level increase for Nb-doped structures, the growth is not so significant and one can observe also slight decrease of m_e^* for higher doped structure (this is in very good agreement with experimental results presented in next paragraph for conductivity measurements carried out in synthetic air atmosphere – Fig. 7).

Electrical properties

Oxidizing conditions. The electrical properties of $SrTi_{1-x}Nb_xO_3$ samples were examined in the oxidizing (synthetic air mixture) and reducing (10% H_2/90% Ar) atmospheres. The defects structure in the studied system is essential to determine the mechanism of conductivity. These considerations should begin with the case of undoped samples synthesized in air atmosphere, therefore the conductivity measurements were carried out first in such atmosphere. Due to naturally occurring vacancies (V''_{Sr}, V''''_{Ti} and $V^{\cdot\cdot}_{O}$) in undoped $SrTiO_3$ obtained during synthesis in air atmosphere, this material is known as acceptor-doped system. The hole carriers at lower temperatures (below 550 K according to[42]) are created as a consequence of ionization of strontium vacancies:

$$V^{\times}_{Sr} = V'_{Sr} + h^{\cdot} \text{ and next } V'_{Sr} = V''_{Sr} + h^{\cdot} \quad (1)$$

and, at higher temperatures, through oxygen incorporation into $SrTiO_3$ structure according to the following equation:

$$\frac{1}{2}O_{2(g)} + V^{\cdot\cdot}_{O} = O^{\times}_{O} + 2h^{\cdot} \quad (2)$$

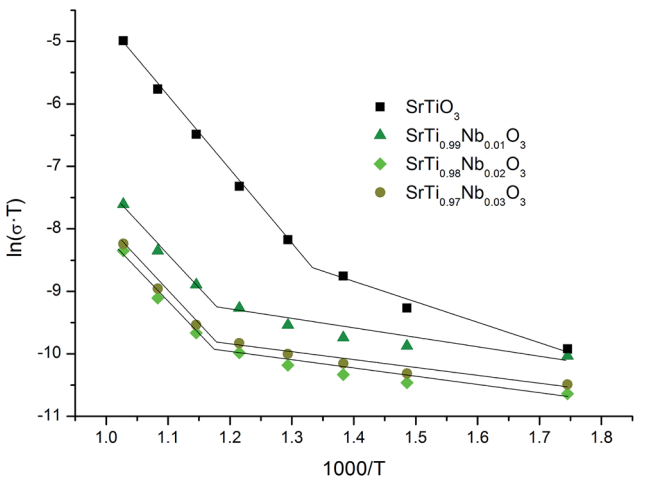

Fig. 7 Temperature dependence of the total conductivity of samples measured in synthetic air atmosphere.

Open Access Article. Published on 01 June 2017. Downloaded on 2/11/2026 10:26:06 AM. This article is licensed under a Creative Commons Attribution-NonCommercial 3.0 Unported Licence.

Further increase of temperature leads to an equilibrium shift to the left and to change of conduction mechanism as a result of ionic conductivity appearance.

The substitution of niobium in titanium site results in incorporation of additional electrons:

$$Nb_2O_5 \xrightarrow{SrTiO_3} 2Nb_{Ti}^{\cdot} + 2e' + 5O_O^{\times} \quad (3)$$

which can: occupy empty states in conduction band (thus being delocalized and able to recombine with holes in the system); be trapped at titanium sites, which results in Ti^{4+} reduction to Ti^{3+} ions, trapped at oxygen vacancies (which can be described by following equations: (a) $V_O^{\cdot\cdot} = V_O^{\cdot} + e$ and (b) $V_O^{\cdot} = V_O^{\times\cdot} + e$); create small polarons localized at titanium site. The latter effect (with additional, possible introduction of oxygen to the structure) are most probable under oxidizing atmosphere.

Simultaneously with niobium, a larger amount of oxygen (in comparison with undoped $SrTiO_3$ structure) is introduced to the structure. As a consequence the strontium and/or titanium vacancies can be created. According to[43] the formation energy for titanium vacancies is higher than for strontium ones, so the latter are more energetically favorable and the process occurring in air atmosphere can be described by the following equation:

$$\frac{x}{2}Nb_2O_5 + Sr_{Sr}^{\times} + (1-x)Ti_{Ti}^{\times} + (3-2x)O_O^{\times} \rightarrow xNb_{Ti}^{\cdot} + (1-x)Ti_{Ti}^{\times} + Sr_{Sr} + \frac{x}{2}V_{Sr}'' + \left(3+\frac{x}{2}\right)O_O \quad (4)$$

These equations and results of impedance spectroscopy measurements were used to explain the changes in the nature of conductivity in oxidizing (air) atmosphere in undoped and Nb-doped $SrTiO_3$ samples. The analysis of total conductivity (σ) was performed based on Bode plots (not included in this paper) but it should be noted that on Nyquist plots only one circle (in impedance system) can be observed for all series of $SrT_{1-x}Nb_xO_3$ (similar results for undoped and yttrium-doped porous $SrTiO_3$ were reported by us[44] and for undoped nanocrystalline $SrTiO_3$ by Gregori *et al.*[45]). The presence of this type of circles (corresponding to resistor and constant phase element) suggests the participation of ionic conductivity in total conductivity of these samples and therefore, respective activation energies were determined based on temperature dependence of total conductivity in Arrhenius plot $\ln(\sigma T)$ *versus* $1/T$ (Fig. 7). One can observe that conductivity of undoped $SrTiO_3$ is much higher than conductivity of Nb-doped strontium titanate and this difference increases with temperature. The conductivities of $SrTi_{0.98}Nb_{0.02}O_3$ and $SrTi_{0.97}Nb_{0.03}O_3$ samples are almost the same and simultaneously half an order of magnitude lower then conductivity of $SrTi_{0.99}Nb_{0.01}O_3$.

Additionally, for all samples, one can observe two temperature regions (the first – lower and the second – higher, with good linear fit) differing considerably in a slope, which indicates the change in dominating conduction mechanism (electronic to ionic from low to high temperature regions). It is, however, worth to note, that while analogous two temperature regions with different dominating conductivity mechanism were also observed in porous yttrium doped $SrTiO_3$ samples,[44] in the latter case, for high temperature region with dominating ionic conductivity, the addition of admixture resulted in an increase of activation energy, whilst in niobium system this energy decreases. This can be attributed, to a large extent, to structural changes: in Y-doped $SrTiO_3$ the unit cell size decreases while in Nb-doped material increases with the amount of admixture. Since yttrium ionic radius is significantly smaller than strontium one (93 *vs.* 112 pm), which corresponds to slightly higher effective nuclear charge, yttrium ions attract oxygen ions stronger than strontium ones and therefore respective bond lengths are smaller causing slight deformation and (mainly) spatial reorientation of TiO_6 octahedra in a proximity of yttrium admixture. In result, the average interatomic distances decrease and potential barriers related to oxygen diffusion through the structure becomes higher and thus higher activation energies are necessary for the oxygen diffusion. On the other hand, as mentioned earlier, niobium ions are slightly bigger than substituted titanium ones and make bigger octahedra at the expense of corner-shared TiO_6 octahedra (resulting in their distortion), which leads to overall structure expansion, giving more room for oxygen ions to diffuse and thus lowering respective activation energy.

Reducing conditions. Under reduction atmosphere conditions, in undoped $SrTiO_3$ additional oxygen vacancies are formed, according to the following defect equation:

$$O_O^{\times} = \frac{1}{2}O_2 + V_O^{\cdot\cdot} + 2e' \quad (5)$$

After donor doping with niobium, extra electrons are being introduced to the structure (eqn (3)) and electrons originating from both processes can be either delocalized, occupying conduction band states, localized at oxygen vacancies:

$$V_O^{\cdot\cdot} + e' = V_O^{\cdot} \text{ and then } V_O^{\cdot} + e' = V_O^{\times} \quad (6)$$

or reducing titanium ion:

$$Ti_{Ti}^{\times} + e' = Ti_{Ti}' \quad (7)$$

In order to determine the effect of strontium substitution with niobium on conductivity of modified materials in an atmosphere that corresponds to working conditions characteristic for SOFC anodes, the impedance spectroscopy measurements in a mixture of 10% H_2/Ar were carried out. The obtained EIS spectra were analyzed based on Bode plots and total electrical conductivities calculated. The dependence of total conductivity (σ) on temperature inverse (in Arrhenius coordinates) is presented in Fig. 8. It can be observed that for all samples, conductivity increases with temperature and conductivities of doped strontium titanate are much larger than in undoped $SrTiO_3$. Moreover, conductivity of doped material is the highest for 1 mol% Nb samples and is an order of magnitude higher than for 2 and 3 mol% samples (for both being very similar), which, in turn, is also an order of magnitude higher than in undoped strontium titanate. The observed increase of total conductivity for niobium doped $SrTiO_3$ samples in

Open Access Article. Published on 01 June 2017. Downloaded on 2/11/2026 10:26:06 AM.
This article is licensed under a Creative Commons Attribution-NonCommercial 3.0 Unported Licence.

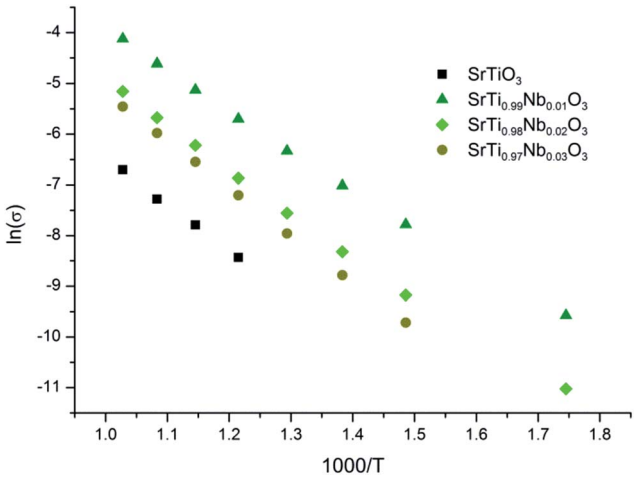

Fig. 8 Temperature dependence of the total conductivity of samples measured in 10% H_2/Ar atmosphere.

reducing atmosphere in comparison with respective values for undoped compound can be attributed to extra electrons coming from niobium, acting as donor dopant (eqn (2)). The drop of conductivity for 2 and 3 mol% samples with respect to 1 mol% sample can be attributed to electron concentration decrease due to the partial localization of electrons coming from oxygen vacancies formation process on niobium cation, which lead to reduction of Nb^{5+} to Nb^{3+}. This can be confirmed by change of samples color from almost white (light cream) before to blue (blue-grey) after reduction process.

It is well known that the conductivity of perovskite materials depends strongly (even a few orders of magnitude) on porosity and the amount of grain boundaries (and thus on grain sizes)[9,46] and therefore our results showing values of total conductivities measured of porous nanocrystalline Nb doped $SrTiO_3$ samples smaller than respective ones obtained for dense microcrystalline samples, are as expected.

Taken together, the observed character of conductivity changes (an increase with temperature), impedance spectra properties (no semicircles in tested frequency range) and theoretical calculations confirm predominant electronic character of conductivity in Nb-doped $SrTiO_3$ for low oxygen partial pressure, so based on $\ln(\sigma)$ *vs.* $1/T$ dependence (Fig. 8) respective conductivity activation energies were determined and are presented in Table 3.

The results indicate that unlike in synthetic air atmosphere, when reducing atmosphere is used, niobium introduction to $SrTiO_3$ structure leads to a drop of conductivity activation energy, which is smallest for $SrTi_{0.99}Nb_{0.01}O_3$ samples and increases back with the increasing amount of niobium added, becoming for $SrTi_{0.97}Nb_{0.03}O_3$ almost identical as for undoped samples.

Chemical stability. The results of the studies on chemical stability of strontium titanate reported in papers referred in introduction gave hope that presented system exhibits high resistance to carbon dioxide and water vapor. To verify this hypothesis with respect to $SrTi_{1-x}Nb_xO_3$ system, undoped and Nb-doped $SrTiO_3$ samples were annealed in CO_2/H_2O atmosphere for four weeks. Next, the fragments of pellets were subjected to thermal analysis with simultaneous analysis of gaseous products by means of mass spectrometry. The thermogravimetry (TG) curves for all samples without exposition on CO_2/H_2O (Fig. 9a) show only traces of mass loss resulting mainly from desorption of a small amount of surface-adsorbed CO_2. The ionic currents corresponding to CO_2 and H_2O ($m/z = 44$ and $m/z = 18$ respectively) hardly changed during the whole measurements for both undoped and doped $SrTiO_3$. Similar effect was observed on both TG and mass spectra in the case of undoped strontium titanate subjected to aging, indicating that the CO_2/H_2O atmosphere practically did not affect the chemical stability of this material. A completely different behavior was observed on TG/MS curves for Nb-doped samples after aging (Fig. 9b). One can observe two separate regions – the first one related to a release of major amount of H_2O and traces of CO_2 (up to around 700 K) and the second one (above 700 K) related only to carbon dioxide evolving (in significantly larger quantities). What is more, low temperature region is not only related to adsorbed water release, but also to some other chemically bonded water (much higher ionic currents corresponding to H_2O were measured for samples after aging in comparison to samples not subjected to aging procedure). On the other hand, in the case of carbon dioxide the values of ionic current are almost at background level in this range of temperature. Formation of strontium hydroxide hydrate during annealing tests is in our opinion the only possible explanation for the effect observed on TG and ionic currents curves. Unfortunately, due to the fact that strontium hydroxide can be present in several different hydrated forms,[47] we cannot determine the amount of moles of $Sr(OH)_2$ produced. Eventually, however, as a result of thermal analysis measurements this compound decomposes to water and strontium oxide. Furthermore it is clearly visible that mass loss below 700 K increases with the amount of Nb admixture in $SrTi_{1-x}Nb_xO_3$ samples. The second range of sample decomposition (above 700 K) is associated with CO_2 releasing as the only gaseous product (as confirmed mass

Table 3 The calculated activation energy determined for measurements in synthetic air and 10% H_2/Ar atmosphere

		E_a [eV]			
Atmosphere/temperature range		$SrTiO_3$	$SrTi_{0.99}Nb_{0.01}O_3$	$SrTi_{0.98}Nb_{0.02}O_3$	$SrTi_{0.97}Nb_{0.03}O_3$
Air synt.	Low temp.	0.27 ± 0.05	0.12 ± 0.03	0.10 ± 0.02	0.11 ± 0.02
	High temp.	1.03 ± 0.02	0.94 ± 0.11	0.96 ± 0.12	0.95 ± 0.09
10% H_2/Ar all range		0.79 ± 0.01	0.66 ± 0.01	0.71 ± 0.02	0.78 ± 0.01

Open Access Article. Published on 01 June 2017. Downloaded on 2/11/2026 10:26:06 AM.
This article is licensed under a Creative Commons Attribution-NonCommercial 3.0 Unported Licence.

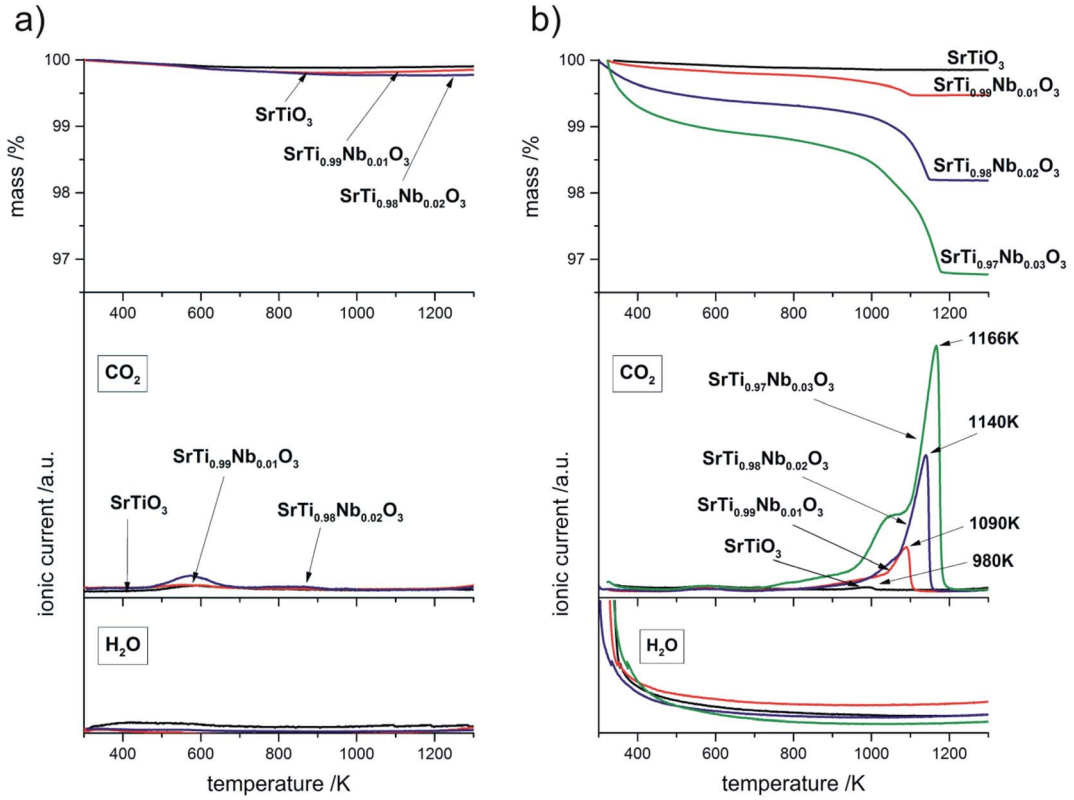

Fig. 9 TG curves and ionic current lines ($m/z = 18$ and $m/z = 44$) for decomposition of $SrTiO_3$ and $SrTi_{1-x}Nb_xO_3$ before (a) and after (b) exposition tests.

spectra) and with mass loss (TG) evidently increasing with niobium content in original samples. This results confirmed formation of some carbonate during aging tests. However, the only possible carbonate that could have formed from the reaction of CO_2 with the elements of the original samples is $SrCO_3$, since neither titanium nor niobium form these compounds. The amount of carbonate produced couldn't be identified by X-ray diffraction (confirmed, however, by Raman spectroscopy measurements – not included here).

Table 4 shows a comparison of CO_2 moles (determined by weight loss on TG curves) resulting from thermal decomposition above 700 K per 1 g of sample with the amount of niobium moles present in 1 g of $SrTi_{1-x}Nb_xO_3$. One can observe that ratio of Nb moles to CO_2 moles systematically decreases, therefore the amount of incorporated Nb indirectly affects the amount of $SrCO_3$ formed. Moreover, thermal decomposition of strontium carbonate begins with destruction of carbonate covering the surface of the nanometric crystallites (Fig. 2) so that the reaction at the surface begins already at about 700 K. The proper effect (running through the whole volume of the resulting grains) begins in undoped sample at 953 K and for the doped samples moves to higher temperatures with increasing amounts of formed carbonate. The shift of the end of the decomposition process towards higher temperatures with the increasing amount of carbonate in the samples (and at the same time with amount of incorporated niobium) is easily noticeable on both, TG and CO_2 ionic currents curves. Described effect is the result of inhibition of the reaction due to CO_2 evolving which at the same time in such porous, nanostructured material becomes the primary constituent of the atmosphere in which this reaction occurs. Thus the reaction equilibria: $SrCO_3 = CO_2 + SrO$ is shifted slightly to the left – the more carbonate is present in the

Table 4 The amount of CO_2 released above 700 K per 1 g of sample (determined by weight loss on TG curves with approx. 5% error) and niobium present in 1 g of $SrTi_{1-x}Nb_xO_3$

Sample	Mass change per 1 g of sample [g]	The number of CO_2 moles produced per 1 g of sample [g]	The number of Nb moles per 1 g of sample [g]	Ratio of Nb moles to CO_2 moles
$SrTi_{0.99}Nb_{0.01}O_3$	1.20×10^{-3}	2.73×10^{-5}	5.44×10^{-5}	1.99
$SrTi_{0.98}Nb_{0.02}O_3$	2.59×10^{-3}	5.87×10^{-5}	1.09×10^{-4}	1.85
$SrTi_{0.97}Nb_{0.03}O_3$	5.22×10^{-3}	1.19×10^{-4}	1.62×10^{-4}	1.37

This journal is © The Royal Society of Chemistry 2017

Open Access Article. Published on 01 June 2017. Downloaded on 2/11/2026 10:26:06 AM.
This article is licensed under a Creative Commons Attribution-NonCommercial 3.0 Unported Licence.

material, the higher partial pressure of CO_2. For better visualization of this shift on Fig. 9b, the temperature of maxima on CO_2 ionic current are appropriately labeled. The most important conclusion that can be drawn from thermal analysis of samples before and post-aging treatment is that niobium introduction to $SrTiO_3$ structure causes decrease of chemical stability of resulting compound.

The experimental results of chemical stability are in opposition to predictions based on earlier cited works.[15,16] Therefore, average metal oxygen bond energy (ABE) were estimated according to the following equation:[17]

$$\mathrm{ABE} = \frac{X_\mathrm{A}}{12m}\left(\Delta H_{\mathrm{A}_m\mathrm{O}_n} - m\Delta H_\mathrm{A} - \frac{n}{2}\times D_{\mathrm{O}_2}\right) + \frac{X_\mathrm{B}}{6m}\left(\Delta H_{\mathrm{B}_m\mathrm{O}_n} - m\Delta H_\mathrm{B} - \frac{n}{2}\times D_{\mathrm{O}_2}\right)$$

where X_A, X_B, $\Delta H_{\mathrm{A}_m\mathrm{O}_n}$ and $\Delta H_{\mathrm{B}_m\mathrm{O}_n}$ are the molar fraction of A-site cation, B-site cation, the heats of formation of $\mathrm{A}_m\mathrm{O}_n$ and $\mathrm{B}_m\mathrm{O}_n$ at 298 K, respectively. D_{O_2} is the oxygen dissociation energy, ΔH_A and ΔH_B are the heats of sublimation of metals A and B at 298 K, respectively. Based on the experimental values of respective enthalpies,[48] the obtained ABE values for $SrTi_{1-x}Nb_xO_3$ ($x = 0$, 0.01, 0.02, 0.03) are equal to (in J mol^{-1}) −392.00, −392.08, −392.17, −392.25, respectively. These values could suggest that niobium substitution for titanium in $SrTiO_3$ structure should result in higher bond strength and therefore increased chemical stability, but in fact, the differences between estimated ABE values are definitely too small to draw such conclusion (especially that this model doesn't take into account local structural deformation which often can result in much higher energy changes). Moreover, this model doesn't take into account also usual formation of additional oxygen vacancies, necessary for overall lattice charge neutralization. Both these factors are – in our opinion – a source of decreased chemical stability of Nb-doped $SrTiO_3$ samples: when oxygen vacancy is introduced to the structure, effective coordination number of respective strontium polyhedra decreases by one and effectively, for slightly increased lengths of Sr–O bonds, their average strength also decreases and so does chemical stability.

Conclusions

Wet synthesis – sol–gel method allowed to obtained porous, nanocrystalline, single phase $SrTi_{1-x}Nb_xO_3$ ($x = 0.0$, 0.01, 0.02, 0.03) materials with all nominal amount of niobium incorporated to structure. The introduction of niobium admixture results in an increase of unit cell volume and simultaneously decrease of average crystallite size (with increasing amount of niobium). The observed changes in structural parameters are in very good agreement with theoretical calculations. QTAiM topological analysis of electron density show that all bonds have significant ionic character, Ti–O and Nb–O bonds are much stronger than Sr–O and small unit cell size expansion with increasing amount of niobium results mostly from deformation of titanium octahedra in niobium proximity in order to relax the structure with longer Nb–O bonds, while TiO_6 octahedra lying further from niobium sites remain practically intact.

The results of aging tests carried out in CO_2/H_2O atmosphere for several weeks showed a worsening of chemical stability with increasing amount of niobium dopant. This can be a result of effective Sr–O bonds weakening in the structure due to titanium octahedral deformation in niobium cations proximity and oxygen vacancies introduction in order to neutralize additional negative charge due to Nb donor doping. To our knowledge, no such tests for this type of the system were carried out earlier.

The electronic structure calculations show that niobium introduction into titanium sublattice has donor character and results in a shift of Fermi level to conduction band (n-type conductor) and small change in band gap size, increasing with niobium amount. The calculated effective electron masses increase with dopant amount, which suggests a lowering of the electric conductivity (in agreement with experimental results obtained for air atmosphere). In reducing atmosphere the total conductivity increases with the amount of admixture, which is a result of additional carriers introduced with oxygen vacancies. To absolute values of the total conductivity measured in reducing atmosphere are significantly lower than reported for other Nb-doped $SrTiO_3$ materials, but this is simply due to completely different microstructure of those materials (highly dense, microcrystalline materials).

Acknowledgements

This work was financially supported by the National Science Center of the Republic of Poland, Grant No. 2014/14/E/ST5/00763. FP-LAPW calculations were supported in part by PL-GRID infrastructure.

References

1 S. Suthirakun, G. Xiao, S. C. Ammal, F. Chen, H.-C. Loye and A. Heyden, *J. Power Sources*, 2014, **245**, 1.
2 J. B. Goodenough and Y.-H. Huang, *J. Power Sources*, 2007, **173**, 1.
3 A. Kulkarni, F. T. Ciacchi, S. Giddey, C. Munnings, S. P. S. Badwal, J. A. Kimpton and D. Fini, *Int. J. Hydrogen Energy*, 2012, **37**, 19092.
4 N. Wang, H. Chen, H. He, W. Norimatsu, M. Kusunoki and K. Kumoto, *Sci. Rep.*, 2013, **3**, 3449.
5 A. V. Kovalevsky, M. H. Aguirre, S. Populoh, S. G. Patricio, N. M. Ferreira, S. M. Mikhalev, D. P. Fagg, A. Weidenkaffh and J. R. Fradea, *J. Mater. Chem. A*, 2017, **5**, 3909.
6 P. Blennow, A. Hagen, K. K. Hansen, L. R. Wallenberg and M. Mogensen, *Solid State Ionics*, 2008, **179**, 2047.
7 B. Bochentyn, J. Karczewski, T. Miruszewski, A. Krupa, M. Gazda, P. Jasinski and B. Kusz, *Solid State Ionics*, 2012, **225**, 118.
8 T. Kolodiazhnyi and A. Petric, *J. Electroceram.*, 2005, **15**, 5.
9 J. C. C. Abrantes, J. A. Labrincha and J. R. Frade, *Sens. Actuators, B*, 1999, **56**, 198.
10 J. Karczewski, B. Riegel, M. Gazda, P. Jasinski and B. Kusz, *J. Electroceram.*, 2010, **24**, 326.
11 G. Sukhdeep, R. Kannan, N. Maffei and V. Thangadurai, *RSC Adv.*, 2013, **3**, 3599.

Open Access Article. Published on 01 June 2017. Downloaded on 2/11/2026 10:26:06 AM.
This article is licensed under a Creative Commons Attribution-NonCommercial 3.0 Unported Licence.

12 P. Pasierb, E. Drożdż-Cieśla, R. Gajerski, S. Łabuś, S. Komornicki and M. Rękas, *J. Therm. Anal. Calorim.*, 2009, **96**, 475.
13 A. Lacz, *Ionics*, 2016, **22**, 1405.
14 E. Drożdż, Ł. Łańcucki and A. Łącz, *J. Therm. Anal. Calorim.*, 2016, **125**, 1225.
15 F. Wang, T. Nakamura, K. Yashiro, J. Mizusaki and K. Amezawa, *Solid State Ionics*, 2014, **262**, 719.
16 L. Gui, Y. Wan, R. Wang, Z. Wang, B. He and L. Zhao, *J. Alloys Compd.*, 2015, **644**, 788.
17 R. J. H. Voorhoeve, J. P. Remeika and L. E. Trimble, *The Catalytic Chemistry of Nitrogen Oxides*, ed. R. L. Klimish and J. G. Larson, Plenum Publishing Cooperation, New York, 1971, p.145.
18 J. D. R. Tilley, *Perovskites Structure-Properties Relationships*, John Wiley & Sons, United Kingdom, 2015.
19 R. I. Eglitis, *Int. J. Mod. Phys. B*, 2014, **28**, 1430009.
20 S. Piskunov, E. Heifets, R. I. Eglitis and G. Borstel, *Comput. Mater. Sci.*, 2004, **29**, 165.
21 R. I. Eglitis, S. Piskunov, E. Heifets, E. Kotomin and G. Borstel, *Ceram. Int.*, 2004, **30**, 1989.
22 R. I. Eglitis and E. Kotomin, *Phys. B*, 2010, **405**, 3164.
23 A. Hamid, *Appl. Phys. A: Mater. Sci. Process.*, 2009, **97**, 829.
24 C. Zhang, C. L. Wang, J. C. Li, K. Yang, Y. F. Zhang and Q. Z. Wu, *Mater. Chem. Phys.*, 2008, **107**, 215.
25 R. K. Astala and P. D. Bristowe, *Modell. Simul. Mater. Sci. Eng.*, 2004, **12**, 79.
26 M. Djermouni, A. Zaoui, S. Kacimi and B. Bouhafs, *Comput. Mater. Sci.*, 2010, **49**, 904.
27 K. Ozdogan, M. Upadhyay Kahaly, S. R. Sarath Kumar, H. N. Alshareef and U. Schwingenschlogl, *J. Appl. Phys.*, 2012, **111**, 054313.
28 J. Shujuan, Y. Jinliang, S. Guipeng and Z. Yinnü, *J. Semicond.*, 2016, **37**, 072001.
29 P. Delugas, A. Filippetti, M. J. Verstraete, I. Pallecchi, D. Marr and V. Fiorentini, *Phys. Rev. B: Condens. Matter Mater. Phys.*, 2013, **88**, 1.
30 B. R. Sudireddy, P. Blennow and K. Nielsen, *Solid State Ionics*, 2012, **216**, 44.
31 P. Blennow, K. K. Hansen, L. R. Wallenberg and M. Mogensen, *J. Eur. Ceram. Soc.*, 2007, **27**, 3609.
32 P. Blaha, K. Schwarz, G. Madsen, D. Kvasnicka, and J. Luitz, *WIEN2k, An Augmented Plane Wave + Local Orbitals Program for Calculating Crystal Properties*, ed. K. Schwarz, Techn. Universität Wien, Wien, Austria, 2001.
33 J. P. Perdew, A. Ruzsinszky, G. I. Csonka, O. A. Vydrov, G. E. Scuseria, L. A. Constantin, X. Zhou and K. Burke, *Phys. Rev. Lett.*, 2008, **100**, 136406.
34 R. F. W. Bader, *Atoms in Molecules: A Quantum Theory*, Clarendon Press, Oxford, 1990.
35 A. Otero-de-la-Roza, E. R. Johnson and V. Luaña, *Comput. Phys. Commun.*, 2014, **185**, 1007.
36 N. Wang, M. Cao, Z. He, Ch. Diao, Q. Zhang, Y. Zhang, J. Dai, F. Zeng, H. Hao, Z. Yao and H. Liu, *Ceram. Int.*, 2016, **42**, 13593.
37 W. H. Baur, *Acta Crystallogr., Sect. B: Struct. Sci.*, 1974, **30**, 1195.
38 K. Robinson, G. V. Gibbs and P. H. Ribbe, *Science*, 1971, **172**, 567.
39 R. Hoppe, *Z. Kristallogr.*, 1979, **150**, 23.
40 M. Marques, L. K. Teles, V. Anjos, L. M. R. Scolfaro, J. R. Leite, V. N. Freire, G. A. Farias and E. F. da Silva Jr, *Appl. Phys. Lett.*, 2003, **82**, 3074.
41 W. Wunderlich, H. Ohta and K. Koumoto, *Phys. B*, 2009, **404**, 2202.
42 R. A. de Souza, *Adv. Funct. Mater.*, 2015, **25**, 6326.
43 A. A. Crawford and P. Jacobs, *J. Solid State Chem.*, 1999, **144**, 423.
44 E. Drożdż, A. Łącz, A. Koleżyński, A. Mikuła and K. Mars, *Solid State Ionics*, 2017, **302**, 173.
45 G. Gregori, S. Heinze, P. Lupetin, H.-U. Habermeier and J. Maier, *J. Mater. Sci.*, 2013, **48**, 2790.
46 F. Horikiri, L. Q. Han, A. Kaimai, T. Otake, K. Yashiro, T. Kawada and J. Mizusaki, *Solid State Ionics*, 2006, **177**, 2555.
47 R. Dinescu and M. Preda, *J. Therm. Anal.*, 1971, **5**, 465.
48 R. A. Robie, B. S. Hemingway and J. R. Fisher, *Thermodynamic Properties of Minerals and Related Substances at 298.15 K and 1 Bar (105 Pascals) Pressure and at Higher Temperatures*, U.S. Geological Survey Bulletin, 1979, vol. 1452.

This journal is © The Royal Society of Chemistry 2017